

Tipifarnib as a Precision Therapy for *HRAS*-Mutant Head and Neck Squamous Cell Carcinomas **AACR**



Mara Gilardi¹, Zhiyong Wang¹, Marco Proietto², Anastasia Chillà¹, Juan Luis Calleja-Valera³, Yusuke Goto¹, Marco Vanoni⁴, Matthew R. Janes⁵, Zbigniew Mikulski⁶, Antonio Gualberto⁷, Alfredo A. Molinolo¹, Napoleone Ferrara¹, J. Silvio Gutkind¹, and Francis Burrows⁸

ABSTRACT

Tipifarnib is a potent and highly selective inhibitor of farnesyltransferase (FTase). FTase catalyzes the posttranslational attachment of farnesyl groups to signaling proteins that are required for localization to cell membranes. Although all RAS isoforms are FTase substrates, only HRAS is exclusively dependent upon farnesylation, raising the possibility that HRAS-mutant tumors might be susceptible to tipifarnib-mediated inhibition of FTase. Here, we report the characterization of tipifarnib activity in a wide panel of *HRAS*-mutant and wild-type head and neck squamous cell carcinoma (HNSCC) xenograft models. Tipifarnib treatment displaced both mutant and wild-type HRAS from membranes but only inhibited proliferation, survival, and spheroid formation of *HRAS*-mutant cells. *In vivo*, tipifarnib

treatment induced tumor stasis or regression in all six *HRAS*-mutant xenografts tested but displayed no activity in six *HRAS* wild-type patient-derived xenograft (PDX) models. Mechanistically, drug treatment resulted in the reduction of MAPK pathway signaling, inhibition of proliferation, induction of apoptosis, and robust abrogation of neovascularization, apparently via effects on both tumor cells and endothelial cells. Bioinformatics and quantitative image analysis further revealed that FTase inhibition induces progressive squamous cell differentiation in tipifarnib-treated HNSCC PDXs. These preclinical findings support that *HRAS* represents a druggable oncogene in HNSCC through FTase inhibition by tipifarnib, thereby identifying a precision therapeutic option for HNSCCs harboring *HRAS* mutations.

Introduction

Squamous cell carcinoma of the head and neck (HNSCC) is the sixth most common cancer worldwide, with an estimated annual incidence of 600,000 patients. In the United States, 55,000 new cases are diagnosed each year, leading to nearly 13,000 deaths annually (1). Early-stage HNSCC disease is treated relatively well with single-modality therapy (either surgery or radiation), but nearly 66% of patients present with advanced disease and fewer than 30% of these patients are cured. Few drugs have proven effective in HNSCC therapy. Systemic, platinum-based chemotherapy is the mainstay of first-line treatment, and combination with 5-FU and the anti-EGFR antibody cetuximab has been shown to extend overall survival in the metastatic setting (2). However, despite

significant advances in the understanding of the molecular underpinnings of this group of tumors, cetuximab was the only molecularly targeted drug approved for HNSCC until the arrival of anti-PD-1 antibodies in 2016, and checkpoint inhibitors only produce durable responses in a minority (<15%–20%) of patients (3). Thus, identification and exploitation of novel druggable oncogenes in HNSCC is urgently needed to improve patient outcomes.

Farnesyltransferase (FTase) is a cytosolic metalloenzyme that catalyzes the transfer of a 15-carbon farnesyl lipid moiety to a group of cellular proteins characterized by a C-terminal CAAX motif (4). Farnesylation is required for cellular membrane insertion and subsequent activity of certain signaling proteins associated with cancer progression (5), spurring the development of several FTase inhibitors (FTI) in the late 1990s and early 2000s. The first selective FTI to enter clinical studies was tipifarnib (R115777), a heterocyclic nonpeptidomimetic drug that inhibits farnesylation of the canonical FTase substrate lamin A with subnanomolar potency (6). The clinical development of tipifarnib began in 1997 and consisted of more than 70 clinical oncology and hematology studies. Many RAS family proteins are farnesylated at steady state, so FTIs were originally conceived as KRAS inhibitors and tested in high-prevalence KRAS-driven tumors. However, it was subsequently discovered that certain farnesylated proteins, including KRAS and NRAS, can be rescued from membrane displacement in the presence of FTIs by an alternative prenylation pathway mediated by the enzyme geranylgeranyl transferase, so clinical activity of tipifarnib and other FTIs in KRAS- and NRAS-driven cancer was modest. In contrast, the third family member, HRAS, is not a substrate for the geranylgeranylated transferase, and its membrane localization and cellular function are suppressed by FTIs (7).

HRAS was originally identified as an oncogene in chemical carcinogenesis studies of skin squamous cell carcinoma (SCC), and recent genomic analyses reveal that it is the predominant mutated RAS isoform in SCCs of several types, including HNSCC (8). The Cancer

¹Moore's Cancer Center, University of California San Diego, La Jolla, California.

²Section of Molecular Biology, Division of Biological Sciences, University of California San Diego, La Jolla, California. ³Cancer Biology and Immunotherapies Group, Sanford Research, Sioux Falls, South Dakota. ⁴Department of Biotechnology and Biosciences, and SYSBIO Centre of Systems Biology, University Milano-Bicocca, Milan, Italy. ⁵Kumquat Biosciences, Inc., San Diego, California.

⁶La Jolla Institute for Allergy and Immunology, Division of Inflammation Biology, La Jolla, California. ⁷Kura Oncology, Inc., Cambridge, Massachusetts. ⁸Kura Oncology, Inc., San Diego, California.

Note: Supplementary data for this article are available at Molecular Cancer Therapeutics Online (<http://mct.aacrjournals.org/>).

M. Gilardi and Z. Wang contributed equally to this article.

Corresponding Authors: J. Silvio Gutkind, University of California San Diego, 3855 Health Sciences Drive, #0803, La Jolla, CA 92093. Phone: 858-534-5980; E-mail: sgutkind@ucsd.edu; and Francis Burrows, Kura Oncology, Inc., San Diego, California. E-mail: francis@kuraoncology.com

Mol Cancer Ther 2020;19:1784–96

doi: 10.1158/1535-7163.MCT-19-0958

©2020 American Association for Cancer Research.

Genome Atlas (TCGA) reports that *HRAS* is mutated in 6% of HNSCC at initial diagnosis (9), and higher frequencies have been reported in some demographic groups associated with exposure to specific oral carcinogens (10). In addition, *HRAS* mutations have been reported in 15% of patients during acquisition of resistance to cetuximab therapy (11).

Prior to a recent report of tipifarnib activity in *HRAS*-mutant thyroid carcinoma (12), historical studies of FTIs in *HRAS*-mutant settings have employed the bladder carcinoma line T24 (6, 13), breast cancer lines (14), or recombinant models (6, 14, 15). Here, we report an in-depth characterization of the antitumor activity of tipifarnib in a series of cell line- and patient-derived HNSCC xenograft models that capture the genomic diversity of this patient subset. Tipifarnib displaced *HRAS* from cellular membranes and selectively inhibited proliferation and survival of *HRAS*-mutant HNSCC cells *in vitro*. In xenograft models, tipifarnib blocked tumor growth and induced regressions in cell line- and early passage patient-derived HNSCCs and was associated with robust inhibition of MAPK pathway signaling downstream of activated *HRAS*. FTI treatment also blocked neovascularization, in part via *HRAS*-independent mechanisms, and analysis of gene expression changes following tipifarnib treatment of *HRAS*-mutant patient-derived xenograft (PDX) models confirmed a robust G₁-S cell-cycle block downstream of MAPK pathway inhibition and revealed induction of squamous lineage differentiation *in vivo*.

Materials and Methods

Cell lines and tissue culture

Human head and neck cancer cell lines CAL27, DETROIT562 (*HRAS* wild type), HN31, and UMSCC17B (*HRAS* mutant) were collected as part of the NIDCR Oral and Pharyngeal Cancer Branch cell collection and have been described previously (16, 17). The novel cell lines ORL48 (*HRAS* wild type) and ORL214 (*HRAS* mutant) were generously provided by Dr. Sok Ching Cheong (Cancer Research Malaysia, Subang Jaya, Selangor, Malaysia). To ensure consistency in cell identity, all the cell lines underwent DNA authentication by multiplex STR profiling (Genetica DNA Laboratories, Inc.) prior to experiments. No *Mycoplasma* was detected through Mycoplasma Detection Kit-QuickTest from Biomake. See Supplementary Materials for additional details.

Tipifarnib

Tipifarnib was provided by Kura Oncology. See Supplementary Materials for drug storage and preparation *in vitro* and *in vivo*.

In vivo mouse experiments and analysis

Studies on cell line-derived HNSCC xenografts were performed at the University of California, San Diego (San Diego, CA), under protocol ASP # S15195, approved by the Institutional Animal Care and Use Committee (IACUC). See Supplementary Materials for additional details. For PDX establishment, fresh surgically removed tumor tissues were obtained by Crown Bio (Crown Bioscience SPF facility; ref. 18) from patients diagnosed as HNSCC with approval by the Institutional Review Boards of the hospital and informed consents from patients, and studies were conducted in accordance with recognized ethical guidelines. The protocol and any amendment(s) or procedures involving the care and use of animals were approved by the Institutional Animal IACUC of CrownBio prior to conduct. During the study, the care and use of animals was conducted in accordance with the regulations of the Association for Assessment and Accreditation of Laboratory Animal Care.

RNAi, cell growth assays, 3D spheroids assay, immunoblot analysis, IHC and immunofluorescence, microfluidic vasculogenesis assay

See Supplementary Materials for additional details.

HRAS plasma membrane translocation assays

For *HRAS*-GFP transfection, cells were grown on μslide glass bottom (ibidi). Cells were transfected with *HRAS*-GFP and the next day were treated with tipifarnib for 48 hours, and the image acquisition was performed by confocal microscopy.

Mouse choroidal explant assay

Male C57BL/6J mice (age P20) were euthanized and their eyes were immediately enucleated for dissection. After removing the cornea and lens, the peripheral choroid-scleral complex was separated from the retina and cut into approximately 1 mm × 1 mm fragments; then, the mouse choroidal explant assay was performed. See Supplementary Materials for additional details.

RNA sequencing and bioinformatic analysis

HN2579 and HN3504 HNSCC PDX tumors were implanted in groups of three animals as described above and allowed to grow to 350 to 450 mm³, treated for four days with vehicle or tipifarnib (80 mg/kg twice daily), excised, and snap-frozen. To ensure unbiased sampling for each tumor lesion, three fragments in different regions of the tumor were collected by microdissection techniques. See Supplementary Materials for RNA extraction, RNA sequencing, and analysis.

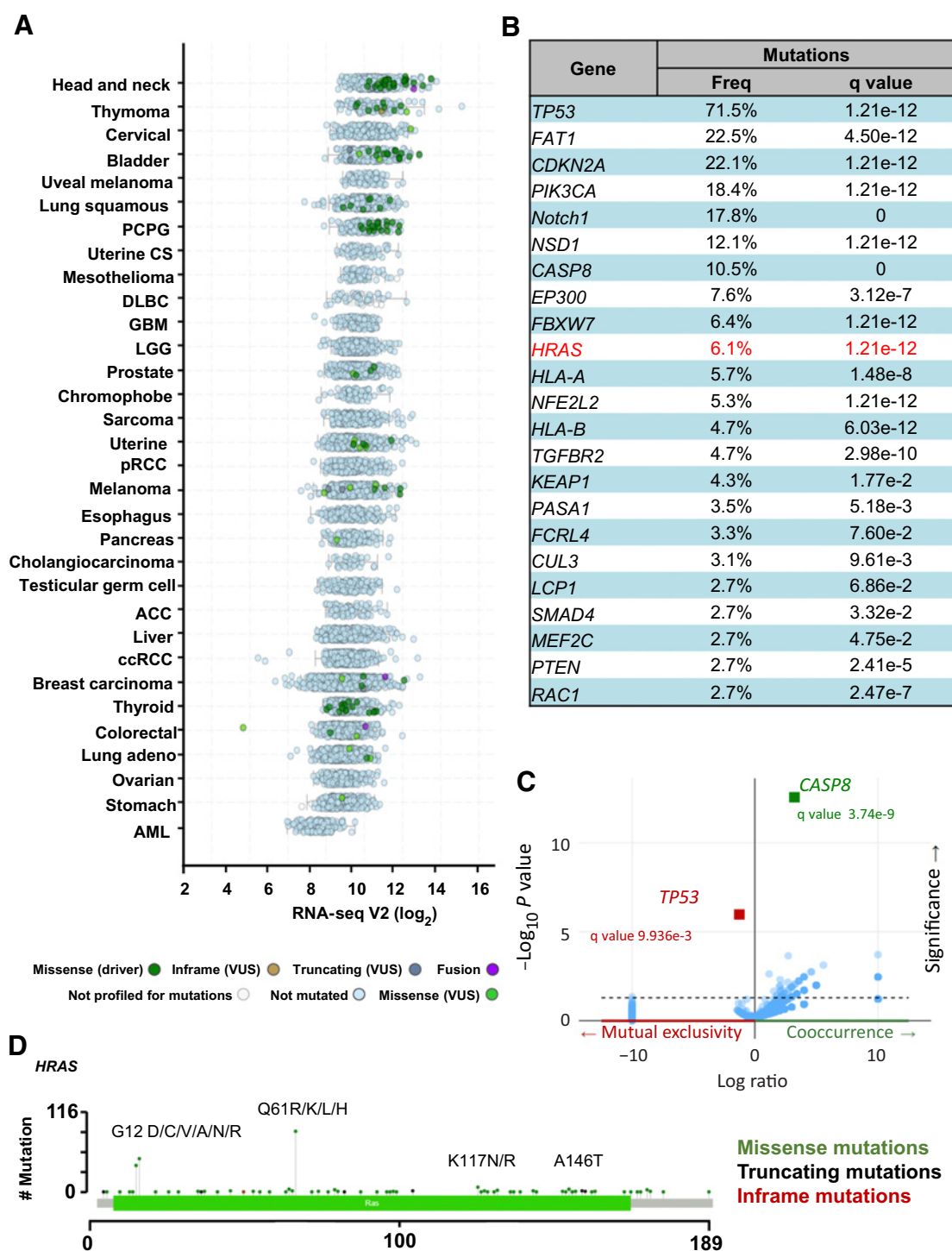
Statistical analysis

GraphPad Prism version 7 for Windows (GraphPad Software) was used to perform data analyses, variation estimation, and validation of test assumptions. The differences between experimental groups in tumor volume, quantification of IHC analysis were performed with longitudinal data analysis method, independent *t* tests, or ANOVA.

Results

Genomics of *HRAS*-mutant HNSCC subset

The recent completion of TCGA (9) has provided an unprecedented opportunity to perform a pancancer analysis of the genomic alterations in *HRAS*. We performed a detailed analysis of genomic information in the TCGA database focused on revealing *HRAS* gene expression levels and mutational status in a broad array of cancer types. This study showed that relatively few cancers harbor *HRAS* mutations, particularly thyroid cancer, pheochromocytoma and paraganglioma (PCPG), and HNSCC (Fig. 1A). Among them, the latter also represents the cancer expressing the highest levels of *HRAS* transcripts, together suggestive of a more prominent role for *HRAS* in this particular cancer type. The TCGA analysis has also provided a comprehensive genomic characterization of HNSCC (Fig. 1B; ref. 9), supporting that *TP53* is one the most mutated genes (71% mutated), followed by *FAT1* (23% mutated), *NOTCH1* (18% mutated), *CASP8* (11% mutated), *CDKN2A* (22% mutated) genes, and *PIK3CA* (~18% mutated; ref. 19). In a prior study, we have performed a pathway-specific analysis of the HNSCC onco-genome, which indicated that the PI3K-mTOR signaling pathway is mutated in the highest percentage of the HNSCC lesions (19). Indeed, *PIK3CA* is the driver oncogene most frequently mutated when considering HPV⁻ and HPV⁺ HNSCC cases (16.8% and 36.1%, respectively; ref. 19). *HRAS* is mutated at a lower frequency

**Figure 1.**

Genomics of *HRAS*-mutant HNSCC subset. **A**, Pan-cancer analysis of the TCGA database focused on *HRAS* gene expression and mutations. Expression level of *HRAS* indicated as \log_2 TPM (transcript count per million) and mutation frequency of *HRAS* (green) across different cancer types in TCGA dataset are represented. **B**, Percentage of samples with one or more mutations in the major driver signaling pathways, including *HRAS*, in HNSCC (TCGA dataset, $n = 523$). Percentage of samples with mutations is indicated, as well as the corresponding statistical significance (q value). **C**, Cooccurrence and mutual exclusivity of *HRAS* mutations in HNSCC (TCGA dataset, $n = 523$). **D**, Mutational plot representing the analysis of cancer-associated *HRAS* mutations from TCGA for HNSCC. The frequency of mutations is depicted by the height of the lollipop.

(6.1%), but only in the HPV⁻ HNSCC group (9), which is often associated with tobacco use and exhibit worse prognosis (9, 20).

HPV infection has been recently recognized as a viral etiologic agent responsible for HNSCC, more specifically in the oropharynx (21, 22). The absence of any *HRAS* mutations in HPV⁺ HNSCC prompted us to explore whether there are other significantly altered genomic alterations concomitant with *HRAS* that may help define better the landscape of *HRAS*-mutant HNSCC. Indeed, aligned with a prior report (23), we found that *HRAS* mutations define a unique subset of HNSCC, characterized, in most of the cases, by coincident loss of function mutations in caspase-8 (q value 3.74×10^{-9}) and enrichment for absence (nearly mutually exclusive) of *TP53* mutations (q value, 9.936×10^{-3} ; **Fig. 1C**). In this regard, *HRAS*-mutant HNSCC cases also

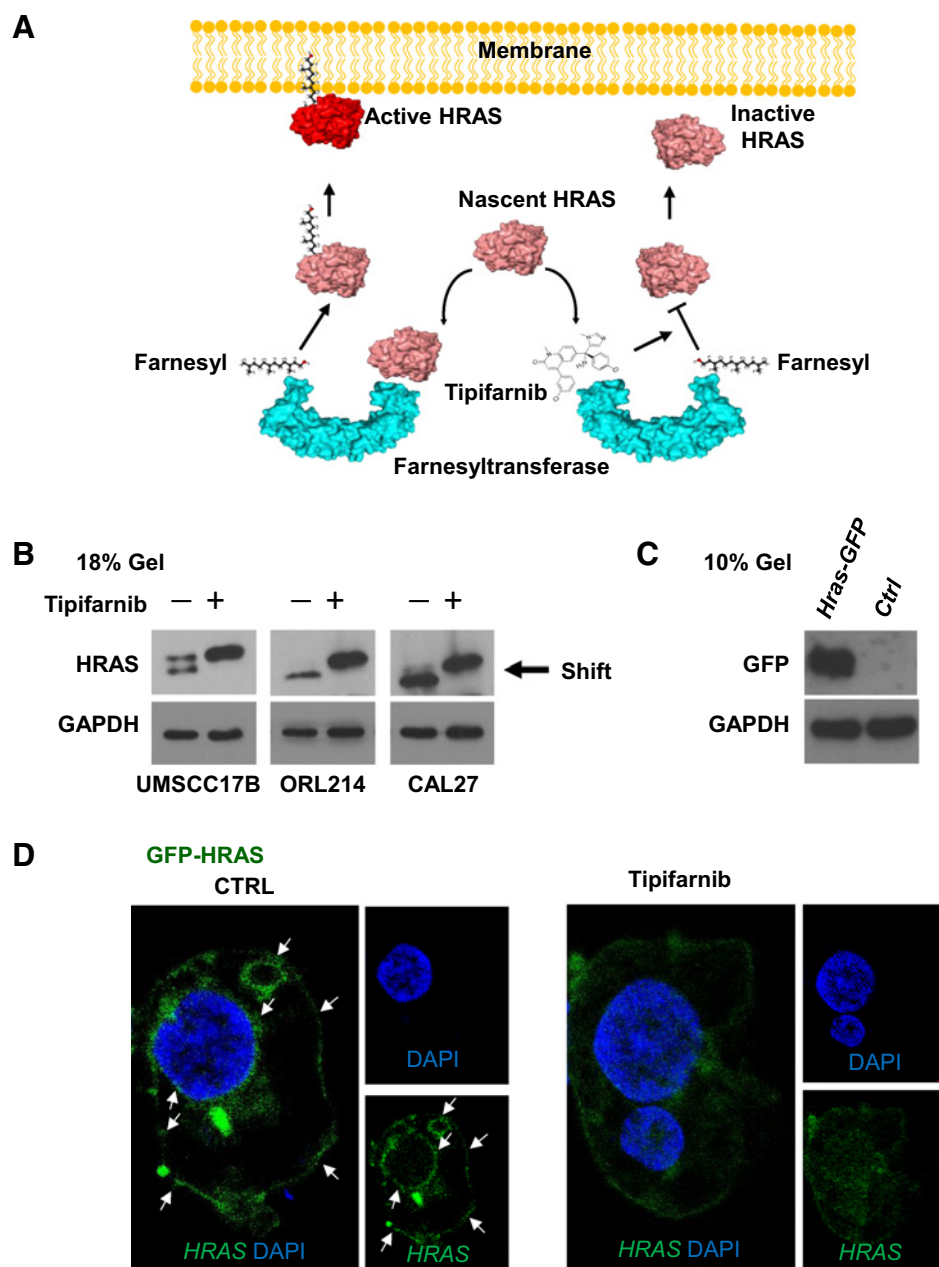
exhibit a low overall mutational burden that is associated with poor response to immuno-oncology agents (9), and hence may instead benefit from the development of targeted options disruption *HRAS* oncogenic signaling. As with the other RAS isoforms, *HRAS* exhibits mutational hotspots in exons 2 (G12, G13), 3 (Q61), and 4 (K117 and A146), but Q61 mutations are more common than in *KRAS* and *NRAS* mutants, where G12 mutations predominate (**Fig. 1D**).

Tipifarnib inhibits *HRAS* farnesylation and displaces it from cellular membranes

RAS proteins are synthesized in the cytosol and subsequent post-translational modifications enable their stable association with intracellular membranes, which is required for GTP hydrolysis and RAS

Figure 2.

Tipifarnib inhibits *HRAS* farnesylation and displaces it from cellular membranes. **A**, Mechanism of action of tipifarnib. RAS proteins are synthesized in the cytosol, and subsequent post-translational modifications enable their stable association with intracellular membranes, which is required for GTP hydrolysis and RAS signaling. *HRAS* is only dependent on farnesylation for its membrane localization. The rate-limiting modification is farnesylation of the cysteine 186, mediated by farnesyltransferase. Tipifarnib displaced *HRAS* from cellular membranes and selectively inhibited proliferation and survival of *HRAS*-mutant HNSCC cells. **B**, Western blot analysis of signaling events in HNSCC cells UMSCC17B, ORL214 (*HRAS* mut), and CAL27 (*HRAS* WT). Cells were cultured in 6-well plates and treated with tipifarnib (200 nmol/L) or DMSO (0.2%) as a control for 48 hours. Western blot analysis was performed in an 18% gel showing that the *HRAS* prenylation shift has been abolished by tipifarnib treatment. **C**, Western blot showing *HRAS*-GFP expression after transfection. **D**, *HRAS* recruitment to the plasma membrane using cells transfected with *HRAS*-GFP. Transfected cells were treated with tipifarnib (200 nmol/L) for 48 hours, and single plan imaging in the center of the cells was performed by confocal microscope allowing fluorescent protein localization.



signaling (4, 5). The rate-limiting modification is farnesylation of the cysteine 186, mediated by farnesyltransferase (Fig. 2A; ref. 24). Because the linkage of a farnesyl moiety to target proteins subtly alters their molecular weight, the so called “farnesylation shift”, we used a high concentration gel (18%) to show that tipifarnib treatment defarnesylated HRAS in both mutant and WT cell lines (Fig. 2B). To determine whether this defarnesylation altered the intracellular trafficking of HRAS protein, we expressed GFP-tagged HRAS in 293 cells (Fig. 2C) to be able to follow its localization with and without tipifarnib treatment. HRAS localized to the plasma and nuclear membranes and membranous organelles in control samples as described previously (25), while tipifarnib-treated cells displayed a more cytosolic localization of the protein (Fig. 2D).

Tipifarnib is selectively cytotoxic to *HRAS*-mutant HNSCC *in vitro*

We characterized the effect of tipifarnib in *HRAS*-mutated and WT human HNSCC cell lines to determine whether the drug was selectively active in the *HRAS*-mutant subset. First, we treated the cells with tipifarnib or knocked down *HRAS* by siRNA, and the effect was verified by Western blot analysis (Fig. 3A). Furthermore, we compared the proliferation of *HRAS*-mutated HNSCC (UMSCC17B and ORL214) with *HRAS* WT (CAL27) treated with siRNA or tipifarnib. Although the inhibition of proliferation was incomplete, both tipifarnib and *HRAS* knockdown significantly reduced the growth of *HRAS*-mutated cell lines, while no significant effects were detected in *HRAS* WT cells (Fig. 3B). *HRAS* knockdown with siRNAs and tipifarnib treatment reduced pERK and pMEK levels in *HRAS*-mutant HNSCC cells, consistent with the inhibition of the *HRAS*–MEK–ERK pathway, but not in *HRAS* WT cells, using the MEK inhibitor trametinib, which inhibited ERK activation in all cells as a control (Fig. 3C).

The initial experiments with tipifarnib and *HRAS* knockdown were performed in monolayer culture, but as several groups have recently reported that this format fails to capture the full potency and selectivity of RAS inhibitors (26), we also tested tipifarnib in a larger panel of *HRAS*-mutant and WT cell lines in 3D spheroid formation assays, measuring effects on viability in terms of metabolic activity (Fig. 3D) and absolute number (Fig. 3E) of 3D tumor spheroids. The broadly active *HRAS* nonselective drugs sunitinib and trametinib were employed as controls. 3D assay treatment lasting 3 weeks evidenced distinct behaviors in different conditions. Tipifarnib displayed dose-dependent inhibition of spheroid viability in *HRAS*-mutant cells only (Fig. 3D) and also selectively reduced the absolute number of colonies (Fig. 3E), suggesting that *HRAS* inhibition depletes tumor-initiating cells. In contrast, sunitinib and trametinib were similarly active in both *HRAS*-mutant and WT HNSCC lines (Fig. 3E).

Tipifarnib is highly active in *HRAS*-mutant HNSCC xenografts

Given that tipifarnib shows selective cytotoxicity to *HRAS*-mutant HNSCC cells *in vitro*, we next asked whether tipifarnib is sufficient to display tumor-suppressive effects *in vivo*. For these studies, we used UMSCC17B cells exhibiting a *HRAS* Q61L mutation and ORL214, which has a *HRAS* G12C mutation. Remarkably, we observed that tipifarnib significantly halted tumor growth from as early as 3 days after treatment initiation ($n = 6$, $P < 0.001$; Fig. 4A–C). Tipifarnib reduced pERK in both xenograft models (Fig. 4D). Moreover, IHC for cleaved caspase-3 and IF for Ki67 showed that the inhibition of *HRAS* by tipifarnib caused increased apoptosis and a reduction of cell proliferation in HNSCC tumors (Fig. 4D).

Activity of tipifarnib in *HRAS* mutant is independent of genotype

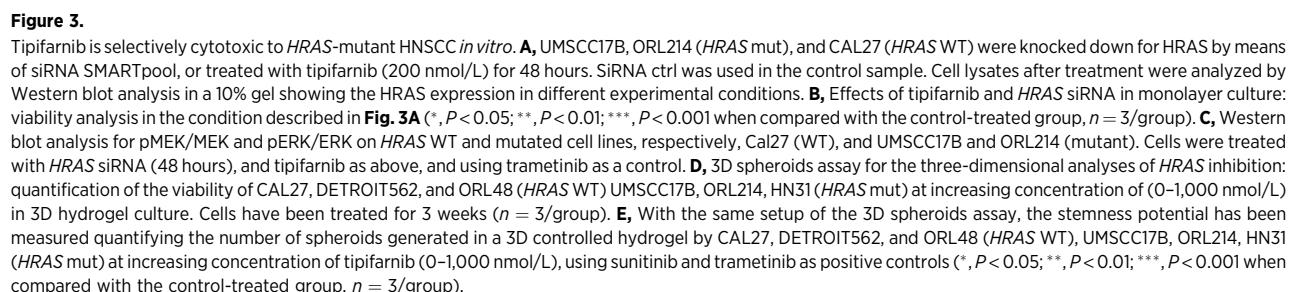
We next extended our analysis to include a panel of *HRAS*-mutant and *HRAS* wild-type patient-derived HNSCC xenograft (PDX) models (Supplementary Fig. S1A), as they may better reflect the complexity of the HNSCC lesions and limit the genetic drift that may occur during establishment and maintenance of HNSCC cell lines *in vitro*. In addition, because widespread differences exist within individual residues and hotspot gene mutations of amino acids and tumor types (27), the expansion of the study to include PDX models increased the range of hotspot mutations to include A146T (HN1420 model), G12S (HN2579), G13R (HN2581), and K117N (HN3504; Fig. 1D). Because tipifarnib is likely to be inhibiting the function of other farnesylated proteins in HNSCC models *in vivo*, it was important to determine whether the presence of mutant *HRAS* was necessary for the robust observed antitumor activity of the drug. As shown in Fig. 5, tipifarnib displayed selective antitumor activity in *HRAS*-mutant HNSCC PDX models. The six *HRAS* wild-type tumors grew progressively while on tipifarnib treatment (Fig. 5A; Supplementary S1B and S1C) but, in sharp contrast, all four *HRAS*-mutant tumors were highly sensitive to tipifarnib when compared with the control-treated groups ($P < 0.01$; Fig. 5A and B), demonstrating that mutant *HRAS* is required for tumor control by tipifarnib in HNSCC models. Consistent with our previous xenograft data, IHC for pERK (Fig. 5C) and IF for Ki67 (Fig. 5D) showed that tipifarnib caused a reduction of ERK activation and cell proliferation in these PDX models. Moreover, as expected, tipifarnib drastically reduced farnesylated proteins (Fig. 5E), and vessel density by CD31 staining (Fig. 5F; ref. 28).

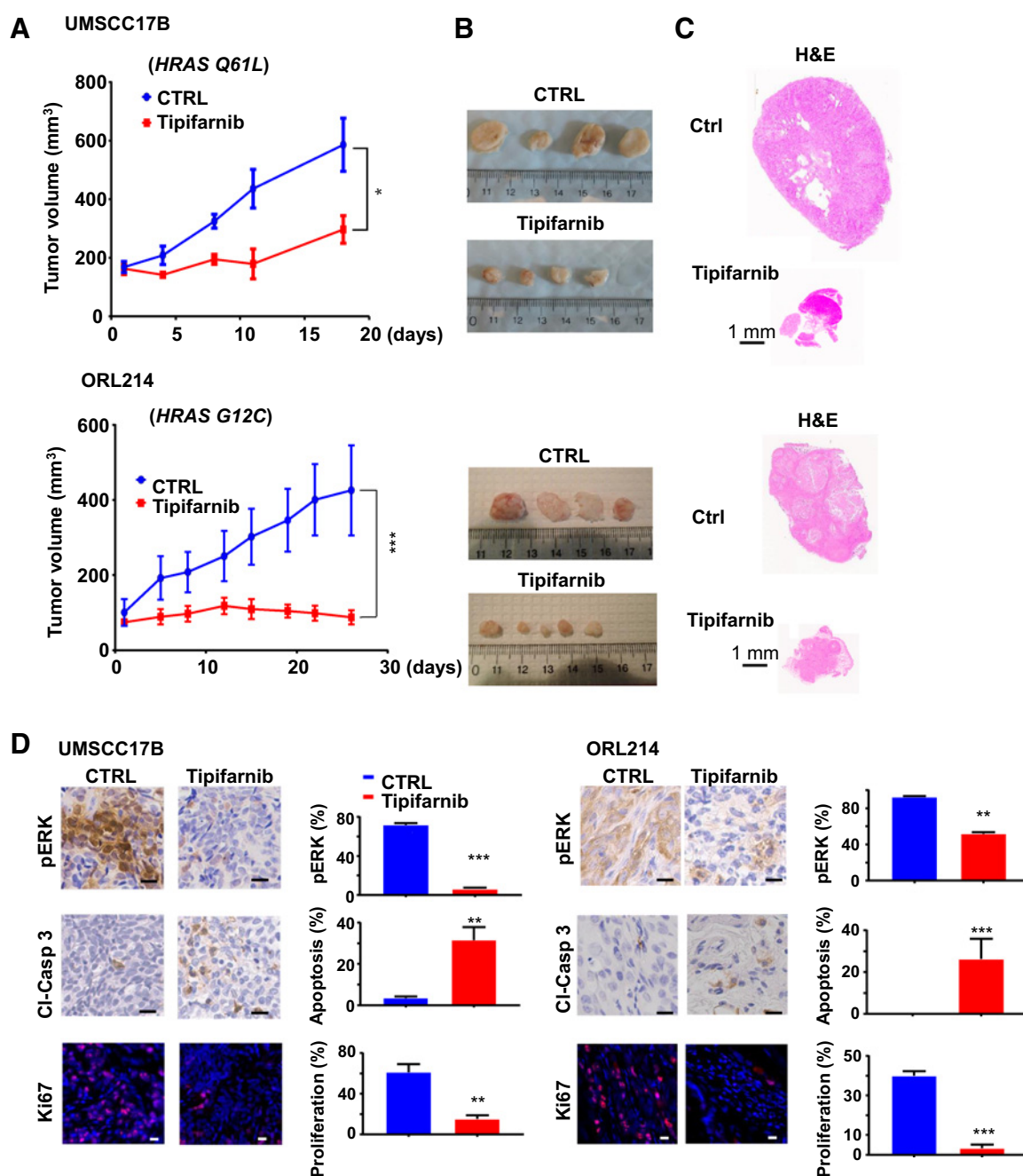
Tipifarnib inhibits angiogenesis and vasculogenesis

Tumors can increase their blood supply by two recognized mechanisms: *de novo* formation of vessels by the differentiation of the endothelial progenitor cells, known as vasculogenesis, and angiogenesis, the sprouting of new blood vessels from the existing vasculature. Previous studies indicated that tipifarnib and other FTIs inhibit tumor angiogenesis (13, 28), but antiangiogenic activity can vary between different tumor types, so we sought to expand these observations in the context of *HRAS*-mutant HNSCC. CD31 immunostaining demonstrated that tipifarnib significantly inhibited vessel formation in both UMSCC17B and ORL214 xenograft tumors (Fig. 6A and B). Moreover, to explore whether tipifarnib may also act on endothelial cells directly, we performed a 3D vasculogenesis assay in a microfluidic model. Briefly, GFP-HUVECs were grown in 3D hydrogel in microfluidic channels for 48 hours with and without tipifarnib. The number of branches was quantified, which revealed the inhibitory effect of tipifarnib on vessel generation (Fig. 6C). Choroid sprouting assay can be used as an *ex vivo* model for studying microvascular angiogenesis. We then tested tipifarnib effects using the choroid sprouting assay. As shown in Fig. 6D, tipifarnib robustly inhibited vessel sprouting from mouse choroid in the 3D matrix, suggesting that both pathological and physiological neovascular processes are sensitive to farnesyltransferase inhibition.

Tipifarnib induces differentiation in patient-derived tumors

To further elucidate the consequences of interfering with mutant *HRAS* and other farnesylated targets in HNSCC, we performed bioinformatics analysis of tipifarnib-induced gene expression changes in PDX models. Two tipifarnib-sensitive *HRAS*-mutant HNSCC PDX models were treated with tipifarnib for 4 days, at which point the tumors were harvested and processed for RNA sequencing. Data were

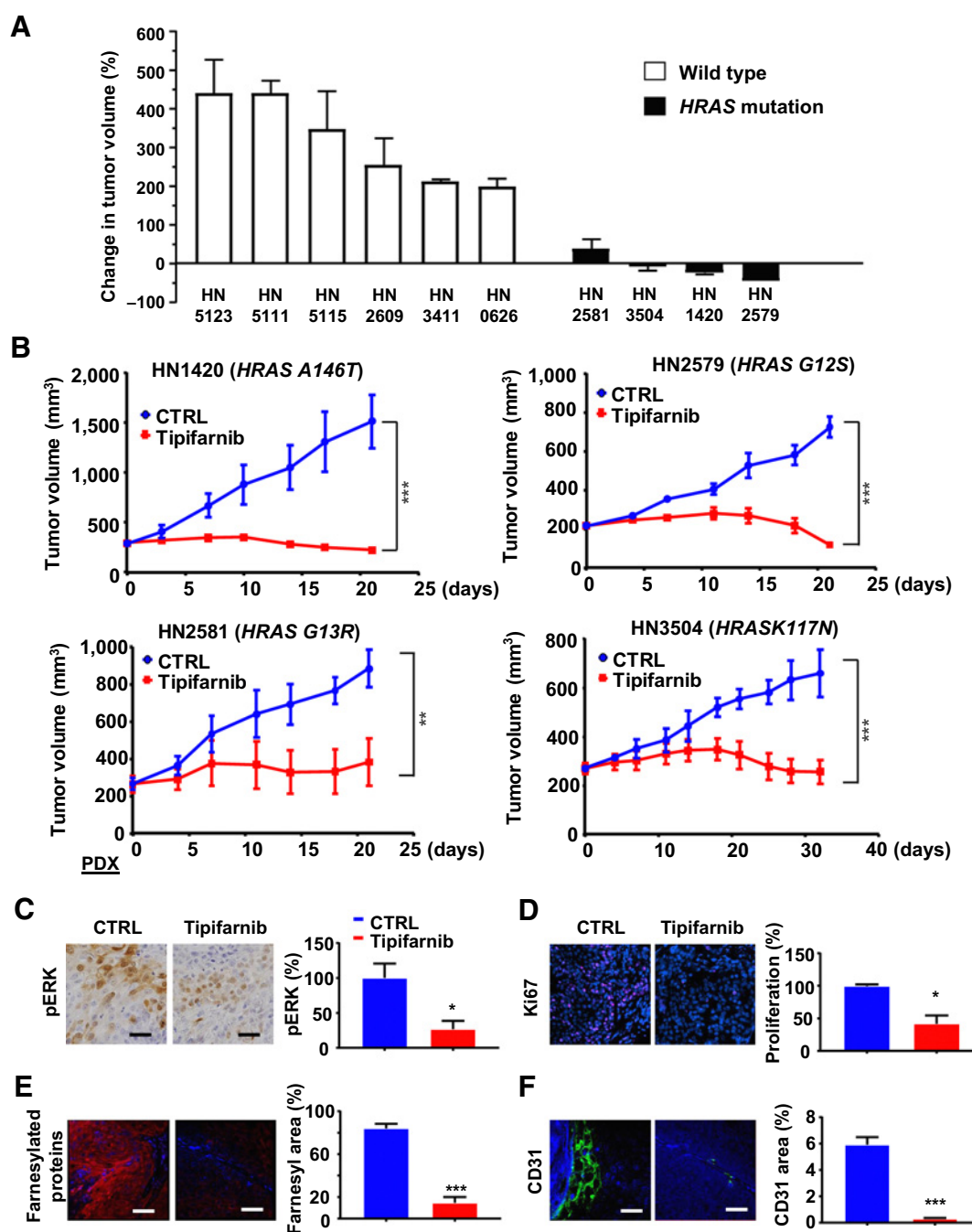


**Figure 4.**

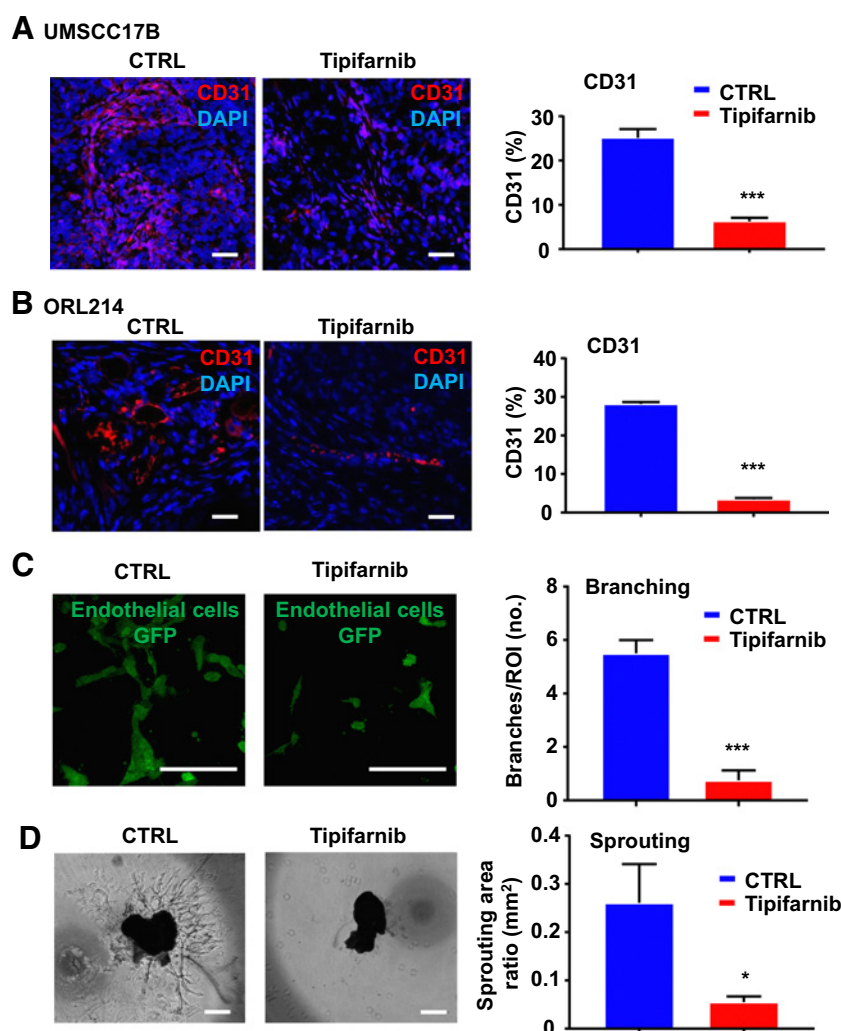
Antitumor activity of tipifarnib in cell line-derived HNSCC xenograft models. **A**, UMSCC17B (top) and ORL214 (bottom) were transplanted into athymic nude mice and NOD/SCID mice, respectively, and treated with vehicle or tipifarnib (60 mg/kg twice daily) as indicated (*, $P < 0.05$; ***, $P < 0.001$ when compared with the control-treated group, $n = 6/\text{group}$). Representative tumor images (**B**) and histologic sections (**C**) from each treatment group in **A**. **D**, Left, representative IHC analysis of pERK and cleaved caspase-3, and representative immunofluorescence analysis of Ki67 in tumors from **A**; Right, quantification from images on the left using QuPath software (*, $P < 0.05$; **, $P < 0.01$; ***, $P < 0.001$ when compared with the control-treated group, $n = 3/\text{group}$).

processed and analyzed using a combination of commercial (Rosalind by OnRamp, Advaita) and Open Source (ENRICH) resources. As shown in **Fig. 7A** and **E**, gene set enrichment analysis (GSEA) revealed two prominent patterns of altered gene expression in tipifarnib-treated tumors. When the two models were analyzed collectively, the predominant changes related to inhibition of cell cycle progression

(**Fig. 7A**, Supplementary Fig. S2, Supplementary Fig. S3), as expected from RAS-MAPK biology. Advaita cell pathway analysis showed that the expression of drivers of G₂-M progression, such as cyclins A and B, CDK1 and CDC25, and mitotic regulators, including BUB1 and PLK1, was suppressed (**Fig. 7B**; Supplementary S2A), consistent with shutdown of RAS-MAPK-cyclin D signaling, the dominant mitogenic

**Figure 5.**

Antitumor activity of tipifarnib in *HRAS*-mutant PDX models. **A**, Waterfall plot of tipifarnib antitumor activity in *HRAS* wild-type and mutant PDX models. The columns in the graph represent the volume change comparing before and after treatment with tipifarnib. Athymic nude mice were inoculated subcutaneously with 2- to 3-mm tumors fragments, the PDXs were allowed to establish to 250 to 350 mm³, and then, the animals were randomized into groups of three and treated orally with vehicle or tipifarnib (60 mg/kg twice daily) for approximately 20 days. **B**, PDX models containing endogenous *HRAS* mutations. HN1420, HN2579, HN2581, and HN3504 fragments were transplanted into athymic nude mice, treated with vehicle or tipifarnib (60 mg/kg twice daily) as indicated (*, $P < 0.05$; **, $P < 0.01$; ***, $P < 0.001$ when compared with the control-treated group, $n = 3$ /group). **C**, Representative IHC or immunofluorescence analysis (left) and quantification using QuPath (right) of pERK (top left), Ki67 (top right), farnesylated proteins (bottom left), and CD31 (bottom right) in PDX samples (*, $P < 0.05$; **, $P < 0.01$; ***, $P < 0.001$ when compared with the control-treated group, $n = 3$ /group). The analyzed samples are related to the HN3504 PDX models using the same treatment as in **A**.

**Figure 6.**

Tipifarnib inhibits angiogenesis *in vitro*, *ex vivo*, and *in vivo*. UMSCC17B (**A**) and ORL214 (**B**) were transplanted into athymic nude mice and NOD-SCID mice, respectively, and treated with vehicle or tipifarnib (60 mg/kg twice daily) as indicated. Representative immunofluorescence analysis (left) and quantification (right) of CD31 in xenograft models. **C**, Vasculogenesis assay in the microfluidic model (left) and quantification (right) of the endothelial cells branching. GFP HUVECs were seeded through microfluidic channels in a 3D environment and treated with tipifarnib 200 nmol/L for 48 hours. Number of branches were quantified in at least 3 ROIs for each condition, and at least 3 microfluidic devices for each condition have been cultured (*, $P < 0.05$; **, $P < 0.01$; ***, $P < 0.001$ when compared with the control-treated group, $n = 3/\text{group}$). **D**, Mouse choroidal explant assay: vessel outgrowth in a mouse choroid explant model in a 3D environment. Representative images of vessel growth after 6 days of incubation with tipifarnib 200 nmol/L (left) and quantification of the sprouting area (right; *, $P < 0.05$; **, $P < 0.01$; ***, $P < 0.001$ when compared with the control-treated group, $n = 3/\text{group}$). no., number.

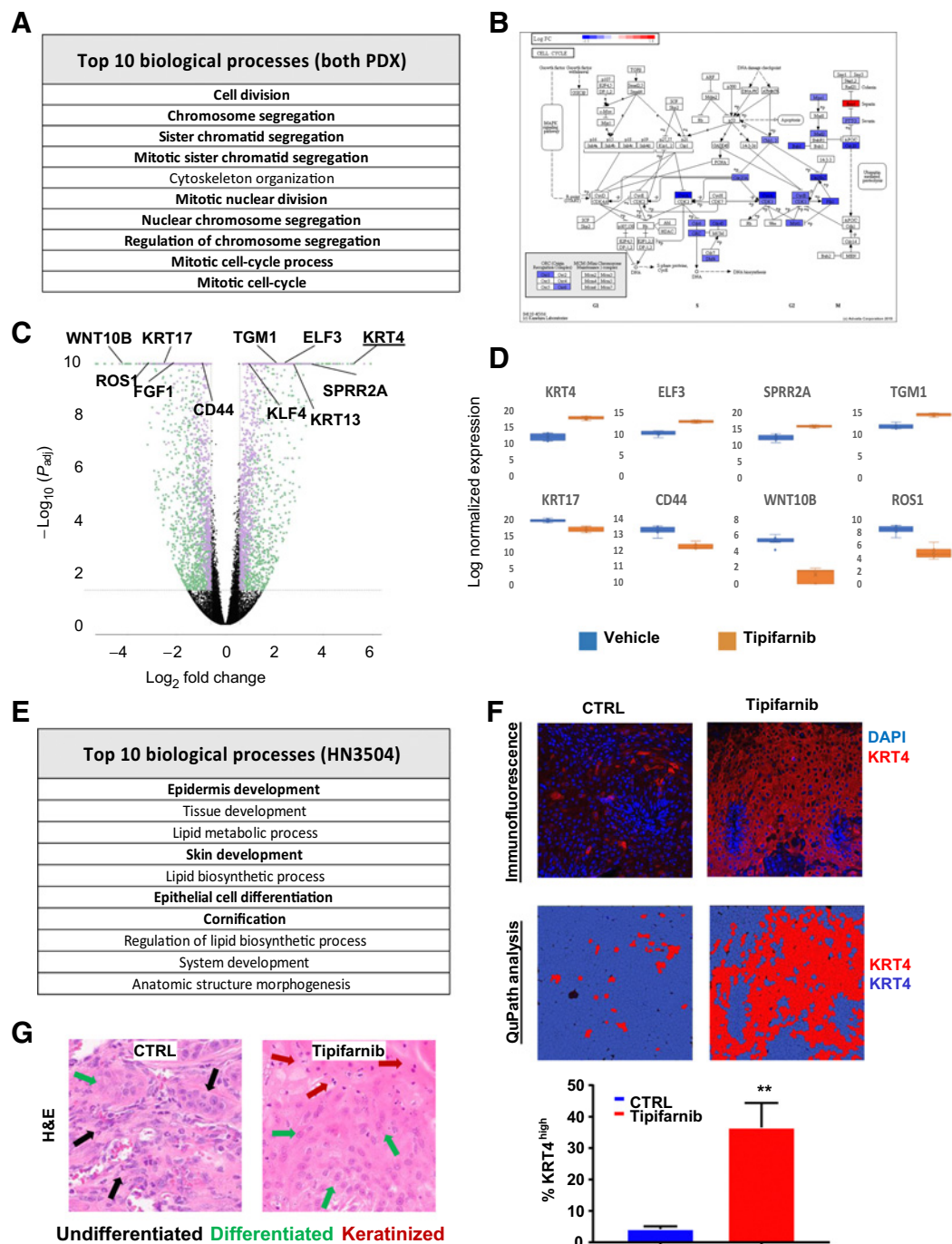
pathway in *HRAS*-mutant cells leading to cell cycle arrest at the G1-S boundary.

However, when the two PDX models were analyzed individually a second prominent transcriptional phenotype emerged in the HN3504 model, where GSEA enriched for processes and pathways associated with differentiation of squamous cells (Fig. 7E), including epidermal development, skin development, epithelial differentiation and cornification. Keratinocytes in stratified squamous epithelia, such as the skin and the lining of the upper aerodigestive tract from which HNSCC is derived, originate as proliferating progenitor cells in the basal layer and progressively differentiate towards specialized post-mitotic cells as they move outward (29). This progression is associated with characteristic alterations in patterns of cytokeratin expression and ultimately enzymatic cross-linking of cellular proteins with barrier function, known as cornification. As shown in the volcano and box and whisker plots of gene expression changes induced by tipifarnib in HN3504 tumors (Fig. 7C and D; Supplementary S2B, Supplementary Table S1), the well-characterized squamous differentiation markers cytokeratin 4 (KRT4) and KRT13 (30), the epithelial differentiation transcription factors ELF3 (31) and KLF4 (32), the cornified protein precursor SPRR2A and the cross-linking enzyme transglutaminase-1 (TGM1) were among the most strongly upregulated loci ($p\text{-Adj } 6.83\text{e-}21 -$

$1.01\text{e-}54$). By contrast, the basal cytokeratin KRT17, the 'stemness' markers CD44 (33) and WNT10B (34) and the HNSCC oncogene ROS1 (35) were all strongly downregulated ($p\text{-Adj } 2.49\text{e-}14 - 9.74\text{e-}22$). Squamous differentiation in tipifarnib treated HN3504 tumors was confirmed histologically by robust staining for KRT4, and by quantitative analysis of the of the immunofluorescence results. Moreover, the presence of characteristic squamous differentiation morphological features in tipifarnib-treated HN3504 tumors is shown in the H&E staining sections (Fig. 7G).

Discussion

RAS genes are the most common driver oncogenes in human cancer, being mutated in approximately one third of cancer cases, so considerable efforts have been made for decades to develop therapeutics for *RAS*-driven tumors (36). Despite this significant investment, no drugs directly targeting *RAS* proteins have been approved, and alternative strategies directed against downstream *RAS* pathways such as MAPK and PI3K have also proved ineffective, primarily due to feedback reactivation via *RAS* (37). Direct inhibition of *RAS* proteins at the catalytic site is impractical due to their picomolar affinity for GTP (37), but a recent breakthrough has enabled direct inhibition of KRAS^{G12C} (26).

Tipifarnib as a Precision Therapy for *HRAS*-Mutant HNSCC**Figure 7.**

Bioinformatics analysis of tipifarnib activity in PDX models. **A**, GSEA of top processes altered by tipifarnib treatment in the combined dataset of HN2579 and HN3504 xenografts. **B**, Advaita pathway diagram illustrating the roles of genes suppressed by tipifarnib treatment in G₂ and M phases of the cell cycle. **C**, Volcano plot of differentially expressed (DE) genes in tipifarnib-treated HN3504 tumors ($n = 3,794$, fold change ≥ 1.5 , $P_{\text{adj}} < 0.05$). Green: less abundant transcripts, purple: more abundant transcripts. **D**, Box and whisker plots of representative highly DE genes in tipifarnib-treated HN3504 tumors. Upregulated genes: KRT4 (fold change, 35.33; $P_{\text{adj}} = 1.01\text{e-}54$), ELF3 (fold change, 6.31; $P_{\text{adj}} = 2.41\text{e-}37$), SPRR2A (fold change, 8.97; $P_{\text{adj}} = 3.52\text{e-}27$), TGM1 (fold change, 6.16; $P_{\text{adj}} = 4.37\text{e-}28$). Downregulated genes: KRT17 (fold change, -5.76; $P_{\text{adj}} = 2.75\text{e-}20$), CD44 (fold change, -2.02; $P_{\text{adj}} = 2.49\text{e-}14$), ROS1 (fold change, -8.86; $P_{\text{adj}} = 4.98\text{e-}21$), WNT10B (fold change, -17.10; $P_{\text{adj}} = 9.74\text{e-}22$). **E**, GSEA of top processes altered by tipifarnib treatment in HN3504 xenografts. **F**, Immunofluorescence (top) and quantification analysis using QuPath software (bottom) of KRT4 expression in control and tipifarnib-treated HN3504 PDX tumors. Red indicates KRT4 HIGH, and blue indicates KRT4 negative. **G**, H&E highlighting morphologic evidence of squamous differentiation in control and tipifarnib-treated HN3504 PDX tumors. BALB/c nu/nu mice were inoculated subcutaneously with 2- to 3-mm tumor fragments, the PDXs were allowed to establish to 250 to 350 mm³, and the animals were randomized into groups of three and treated orally with vehicle or tipifarnib (60 mg/kg twice daily) for approximately 20 days.

The only other currently feasible way to disrupt RAS activity directly is through preventing appropriate intracellular localization by interfering with RAS prenylation (36). Several dozen proteins are farnesylated under basal conditions and tipifarnib treatment blocks their prenylation (38), but inhibition of the farnesylation of KRAS and NRAS leads to compensatory geranylgeranylation and the restoration of membrane localization in the presence of tipifarnib (7, 38). In contrast, HRAS cannot be geranylgeranylated, and its membrane localization and cellular function may be suppressed by FTIs (38, 39). In this study we report that mutant *HRAS* is a targetable oncogene via farnesyltransferase inhibition in a molecularly-defined subset of HNSCC. Tipifarnib displayed robust and consistent antitumor activity in a series of cell line- and patient-derived xenograft models of HNSCC but, in sharp contrast, tipifarnib was devoid of activity in *HRAS* wild type HNSCC cell lines and PDX models *in vitro* and *in vivo*. Remarkably, tipifarnib displayed significant inhibition of tumor growth in *HRAS*-mutant xenografts harboring mutations in exon-2 (G12C, G12S, G13R), exon-3 (Q61L) or exon-4 (K117N, A146T), suggesting that all of these mutants are sufficiently oncogenic to drive full malignancy in HNSCC cells, even though exon-2 and exon-3/4 KRAS mutants have been reported to have differing GTPase activities and biologic functions in other cellular contexts (8, 40).

HRAS protein was de-prenylated in both *HRAS*-mutant and wild type HNSCC cells, as indicated by the gel shift and redistribution from intracellular membranes, but tipifarnib only inhibited spheroid growth of the *HRAS*-mutant UMSCC17B, ORL214 and HN31 cell lines, whereas the cytotoxic multikinase inhibitor sunitinib and the MEK inhibitor trametinib displayed similar activity in both *HRAS* mutant and *HRAS* wild type lines. Genetic depletion of *HRAS* was apparently incompletely effective at inhibiting the proliferation of *HRAS*-mutant HNSCC cells, but this experiment was performed in monolayer culture, and these growth conditions have recently been shown to partially undermine RAS dependence (26). Tipifarnib activity was also blunted under these conditions, underscoring the importance of using appropriate assay formats to interpret RAS dependence.

The expected effects on mitogenic signaling, cell cycle progression and apoptosis downstream of inhibition of oncogenic *HRAS* *in vivo* were observed in both cell-derived xenografts and PDX models. ERK phosphorylation was sharply reduced in UMSCC17B and HN3504, but less so in ORL214, perhaps due to feedback reactivation of the MAP kinase pathway. Indeed, ENRICH analysis of upregulated gene-sets in PDX models following 4 days of tipifarnib therapy revealed evidence of upregulation of canonical MAPK pathway negative regulators (DUSP1, DUSP3) and activation of collateral epithelial cell oncogenic pathways including EGF/EGFR and HER2/HER3 signaling, PIK3CA and PTPN11 (Supplementary Fig. S3). Despite this, all models responded well to tipifarnib treatment and proliferation and apoptosis markers were robustly altered at both early and late timepoints during tipifarnib therapy, suggesting that continuous treatment overwhelmed innate tumor resistance mechanisms and maintained sufficient suppression of oncogenic signaling to block tumor growth in these models. Indeed, the antitumor activity of tipifarnib in all *HRAS*-mutant HNSCC models reported here matches or exceeds that reported with a combination of MAPK and PI3K pathway inhibitors in a *HRAS*-mutant lung cancer model (41).

HRAS is among several dozen obligate farnesylated proteins in cells (38), and analysis of treated PDX tumors indicated almost complete disappearance of the farnesyl moiety, raising the possi-

bility that depletion of additional farnesylated target proteins could enhance the antitumor activity of tipifarnib in *HRAS*-mutant HNSCC. Tipifarnib and other FTIs have previously been shown to possess anti-angiogenic activity (5, 28, 42) mediated by effects on both tumor (42) and endothelial cells (28, 43), and we observed both in this study. The farnesylated proteins involved remain to be identified (44), but the lack of significant effects on tumor growth observed in the panel of *HRAS* wild type PDX strongly suggests that either (a) inhibition of angiogenesis does not provide sufficient therapeutic value in HNSCC (45) or (b) some or all of the anti-vascular effects of tipifarnib *in vivo* are secondary to mutant *HRAS* blockade (46).

Bioinformatics analysis of tipifarnib-induced gene expression changes in two PDX models further elucidated the multifactorial mechanisms of antitumor activity of the drug in *HRAS*-mutant HNSCC *in vivo*. GSEA of the combined dataset confirmed that FTI treatment induced a robust cell-cycle block at the G₁-S boundary and also promoted squamous lineage differentiation. Malignant transformation and terminal differentiation are mutually exclusive processes with opposing effects on cellular proliferation. Carcinogenesis in squamous tissues is associated with impairment of differentiation linked to HPV infection or oncogene activation (47, 48). GSEA of *HRAS*-mutant HN3504 PDX tumors treated for 4 days with tipifarnib revealed that initiation of epithelial differentiation was a prominent early effect of farnesyl transferase inhibition in this model. HNSCC stem cell markers such as CD44 (33) and WNT10B (34, 49) and the basal (proliferative) layer cytokeratin KRT17 (29) were also profoundly suppressed. In contrast, the canonical squamous differentiation markers KRT4 and KRT13 (30), prodifferentiation transcription factors ELF3 (31) and KLF4 (32), and cornification markers like SPRR2A, all of which have been reported to be downregulated in HNSCC, were among the most strongly upregulated genes. This suggests that oncogenic *HRAS* may suppress squamous differentiation in HNSCC and that this can be reversed by tipifarnib treatment.

In the current study, we have characterized the antitumor activity and mechanisms of action of tipifarnib in a large series of HNSCC CDX and PDX models. Tipifarnib displayed robust and selective activity in *HRAS* mutant models harboring all of the known hotspot loci. Collectively, these data demonstrate that mutant *HRAS* represents an actionable oncogene in HNSCC that can be targeted with tipifarnib via inhibition of proliferation and angiogenesis and induction of apoptosis and terminal squamous cell differentiation, resulting in consistent stasis or tumor regression *in vivo*.

Tipifarnib was previously studied in an extensive development campaign consisting of more than 70 clinical trials in a variety of tumor types in the late 1990s and early 2000s without the benefit of methods to enrich for clinical activity such as the use of next-generation sequencing to identify patients with specific driver mutations. Although durable responses were achieved in several cancers, response rates were insufficient to support registrational studies in unselected patient populations. Because its reintroduction into the clinic in 2015, several cohorts of *HRAS*-mutant patients have been treated in a single-arm phase II trial (NCT02383927), with encouraging preliminary findings. As reported in 2018 (45, 50), among 7 evaluable patients with HNSCC, 5 (71%) achieved a confirmed partial response with a median duration of response of 14.1 months. Importantly, no *HRAS*-mutant HNSCC patient experienced an objective response on his last therapy prior to receiving tipifarnib (including platinum, immunotherapy and cetuximab ± chemotherapy regimens). On the basis of these initial encouraging clinical responses, and our current findings, an international, multicenter, open-label,

single-arm study of tipifarnib after failure of platinum-based therapy in recurrent or metastatic HNSCC with *HRAS* mutations with registrational intent, AIM-HN, is currently underway (NCT03719690). Indeed, we expect that our experimental studies in genetically defined HNSCC systems harboring *HRAS* mutations may support the rationale for selectively enrolling patients with *HRAS*-mutant HNSCC in future tipifarnib trials, being represented as a novel precision therapeutic approach for HNSCC based on their oncogenomic landscape.

Disclosure of Potential Conflicts of Interest

M.R. Janes is the director at Kumquat Biosciences Inc. A. Gualberto is the chief medical officer at and has ownership interest (including patents) in Kura Oncology. J.S. Gutkind is a scientific advisory board member at Vividion Therapeutics, Oncocutics, and Domain Therapeutics and reports receiving other commercial research support from Kura Oncology. F. Burrows is the vice president (translational research) at Kura Oncology. No potential conflicts of interest were disclosed by the other authors.

Authors' Contributions

M. Gilardi: Conceptualization, methodology, data curation, formal analysis, writing-original draft, writing-review and editing. Z. Wang: Conceptualization, methodology, data curation, writing-original draft, writing-review and editing. M. Proietto: Methodology, formal analysis, writing-original draft, writing-review and editing. A. Chilla: Methodology, formal analysis. J.L. Calleja-Valera:

Conceptualization, formal analysis, writing-original draft, writing-review and editing. Y. Goto: Data curation. M. Vanoni: Writing-original draft, writing-review and editing. M.R. Janes: Data curation, formal analysis. Z. Mikulski: Methodology, data curation, formal analysis, writing-original draft, writing-review and editing. A. Gualberto: Conceptualization, formal analysis, writing-original draft, writing-review and editing. A.A. Molinolo: Data curation, formal analysis. N. Ferrara: Methodology. J.S. Gutkind: Conceptualization, formal analysis, writing-original draft, writing-review and editing, study supervision. F. Burrows: Conceptualization, data curation, formal analysis, writing-original draft, writing-review and editing, study supervision.

Acknowledgments

This project was supported by National Institute of Dental and Craniofacial Research (NIH/NIDCR) grant 1R01DE026870 to M. Gilardi, Z. Wang, Y. Goto, and J.S. Gutkind; and the NIH grant S10OD021831 to Z. Mikulski. Mara Gilardi was supported by FIRC-AIRC fellowship for abroad (Italian Foundation for cancer research). We thank the Staff of La Jolla Institute Microscopy Core Facility, in particular to Drs. Mcardle, Kiosses and Marcovecchio.

The costs of publication of this article were defrayed in part by the payment of page charges. This article must therefore be hereby marked *advertisement* in accordance with 18 U.S.C. Section 1734 solely to indicate this fact.

Received October 5, 2019; revised April 6, 2020; accepted June 16, 2020; published first July 29, 2020.

References

- Cohen EE, LaMonte SJ, Erb NL, Beckman KL, Sadeghi N, Hutcheson KA, et al. American Cancer Society head and neck cancer survivorship care guideline. *CA Cancer J Clin* 2016;66:203–39.
- Vermorken JB, Mesia R, Rivera F, Remenar E, Kaweck A, Rottey S, et al. Platinum-based chemotherapy plus cetuximab in head and neck cancer. *N Engl J Med* 2008;359:1116–27.
- Chow LQM, Haddad R, Gupta S, Mahipal A, Mehra R, Tahara M, et al. Antitumor activity of pembrolizumab in biomarker-unselected patients with recurrent and/or metastatic head and neck squamous cell carcinoma: results from the phase Ib KEYNOTE-012 expansion cohort. *J Clin Oncol* 2016;34:3838–45.
- Sebt SM. Protein farnesylation: implications for normal physiology, malignant transformation, and cancer therapy. *Cancer Cell* 2005;7:297–300.
- Rowinsky EK, Windle JJ, Von Hoff DD. Ras protein farnesyltransferase: a strategic target for anticancer therapeutic development. *J Clin Oncol* 1999;17:3631–52.
- End DW, Smets G, Todd AV, Applegate TL, Fuery CJ, Angibaud P, et al. Characterization of the antitumor effects of the selective farnesyl protein transferase inhibitor R115777 in vivo and in vitro. *Cancer Res* 2001;61:131–7.
- Whyte DB, Kirschmeier P, Hockenberry TN, Nunez-Oliva I, James L, Catino JJ, et al. K- and N-Ras are geranylgeranylated in cells treated with farnesyl protein transferase inhibitors. *J Biol Chem* 1997;272:14459–64.
- Li S, Balmain A, Counter CM. A model for RAS mutation patterns in cancers: finding the sweet spot. *Nat Rev Cancer* 2018;18:767–77.
- Hoadley KA, Yau C, Hinoue T, Wolf DM, Lazar AJ, Drill E, et al. Cell-of-origin patterns dominate the molecular classification of 10,000 tumors from 33 types of cancer. *Cell* 2018;173:291–304.
- Su SC, Lin CW, Liu YF, Fan WL, Chen MK, Yu CP, et al. Exome sequencing of oral squamous cell carcinoma reveals molecular subgroups and novel therapeutic opportunities. *Theranostics* 2017;7:1088–99.
- Braig F, Voigtlaender M, Schieferdecker A, Busch CJ, Laban S, Grob T, et al. Liquid biopsy monitoring uncovers acquired RAS-mediated resistance to cetuximab in a substantial proportion of patients with head and neck squamous cell carcinoma. *Oncotarget* 2016;7:42988–95.
- Untch BR, Dos Anjos V, Garcia-Rendueles MER, Knauf JA, Krishnamoorthy GP, Saqena M, et al. Tipifarnib inhibits *HRAS*-driven dedifferentiated thyroid cancers. *Cancer Res* 2018;78:4642–57.
- Cohen-Jonathan E, Evans SM, Koch CJ, Muschel RJ, McKenna WG, Wu J, et al. The farnesyltransferase inhibitor L744,832 reduces hypoxia in tumors expressing activated H-ras. *Cancer Res* 2001;61:2289–93.
- Lee KH, Koh M, Moon A. Farnesyl transferase inhibitor FTI-277 inhibits breast cell invasion and migration by blocking H-Ras activation. *Oncol Lett* 2016;12:2222–6.
- Kohl NE, Omer CA, Conner MW, Anthony NJ, Davide JP, deSolms SJ, et al. Inhibition of farnesyltransferase induces regression of mammary and salivary carcinomas in ras transgenic mice. *Nat Med* 1995;1:792–7.
- Amornphimoltham P, Patel V, Sodhi A, Nikitakis NG, Sauk JJ, Sausville EA, et al. Mammalian target of rapamycin, a molecular target in squamous cell carcinomas of the head and neck. *Cancer Res* 2005;65:9953–61.
- Wang Z, Martin D, Molinolo AA, Patel V, Iglesias-Bartolome R, Degese MS, et al. mTOR co-targeting in cetuximab resistance in head and neck cancers harboring PIK3CA and RAS mutations. *J Natl Cancer Inst* 2014;106:dju215.
- Guo S, Qian W, Cai J, Zhang L, Wery JP, Li QX. Molecular pathology of patient tumors, patient-derived xenografts, and cancer cell lines. *Cancer Res* 2016;76:4619–26.
- Iglesias-Bartolome R, Martin D, Gutkind JS. Exploiting the head and neck cancer oncogene: widespread PI3K-mTOR pathway alterations and novel molecular targets. *Cancer Discov* 2013;3:722–5.
- The Cancer Genome Atlas Network. Comprehensive genomic characterization of head and neck squamous cell carcinomas. *Nature* 2015;517:576–82.
- D'Souza G, Kreimer AR, Viscidi R, Pawlita M, Fakhry C, Koch WM, et al. Case-control study of human papillomavirus and oropharyngeal cancer. *N Engl J Med* 2007;356:1944–56.
- Gillison ML, Shah KV. Human papillomavirus-associated head and neck squamous cell carcinoma: mounting evidence for an etiologic role for human papillomavirus in a subset of head and neck cancers. *Curr Opin Oncol* 2001;13:183–8.
- The Cancer Genome Atlas Research Network. Comprehensive genomic characterization of squamous cell lung cancers. *Nature* 2012;489:519–25.
- Sacco E, Spinelli M, Vanoni M. Approaches to Ras signaling modulation and treatment of Ras-dependent disorders: a patent review (2007–present). *Expert Opin Ther Pat* 2012;22:1263–87.
- Santra T, Herrero A, Rodriguez J, von Kriegsheim A, Iglesias-Martinez LF, Schwarzl T, et al. An integrated global analysis of compartmentalized *HRAS* signaling. *Cell Rep* 2019;26:3100–15.
- Janes MR, Zhang J, Li LS, Hansen R, Peters U, Guo X, et al. Targeting KRAS mutant cancers with a covalent G12C-specific inhibitor. *Cell* 2018;172:578–89.
- Chang MT, Asthana S, Gao SP, Lee BH, Chapman JS, Kandath C, et al. Identifying recurrent mutations in cancer reveals widespread lineage diversity and mutational specificity. *Nat Biotechnol* 2016;34:155–63.

28. Scott AN, Hetheridge C, Reynolds AR, Nayak V, Hodivala-Dilke K, Mellor H. Farnesyltransferase inhibitors target multiple endothelial cell functions in angiogenesis. *Angiogenesis* 2008;11:337–46.
29. Koster MI, Roop DR. Mechanisms regulating epithelial stratification. *Annu Rev Cell Dev Biol* 2007;23:93–113.
30. Sakamoto K, Aragaki T, Morita K, Kawachi H, Kayamori K, Nakanishi S, et al. Down-regulation of keratin 4 and keratin 13 expression in oral squamous cell carcinoma and epithelial dysplasia: a clue for histopathogenesis. *Histopathology* 2011;58:531–42.
31. Luk IY, Reehorst CM, Mariadason JM. ELF3, ELF5, EHF and SPDEF transcription factors in tissue homeostasis and cancer. *Molecules* 2018;23:2191.
32. Abrego M, Alvarez R, Paparella ML, Calb DE, Bal de Kier Joffe E, Gutkind JS, et al. Impairing squamous differentiation by Klf4 deletion is sufficient to initiate tongue carcinoma development upon K-Ras activation in mice. *Carcinogenesis* 2014;35:662–9.
33. Baillie R, Tan ST, Itinteang T. Cancer stem cells in oral cavity squamous cell carcinoma: a review. *Front Oncol* 2017;7:112.
34. Rhee CS, Sen M, Lu D, Wu C, Leoni L, Rubin J, et al. Wnt and frizzled receptors as potential targets for immunotherapy in head and neck squamous cell carcinomas. *Oncogene* 2002;21:6598–605.
35. Shih CH, Chang YJ, Huang WC, Jang TH, Kung HJ, Wang WC, et al. EZH2-mediated upregulation of ROS1 oncogene promotes oral cancer metastasis. *Oncogene* 2017;36:6542–54.
36. Cox AD, Fesik SW, Kimmelman AC, Luo J, Der CJ. Drugging the undruggable RAS: mission possible? *Nat Rev Drug Discov* 2014;13:828–51.
37. Stephen AG, Esposito D, Bagni RK, McCormick F. Dragging ras back in the ring. *Cancer Cell* 2014;25:272–81.
38. Storck EM, Morales-Sanfrutos J, Serwa RA, Panyain N, Lanyon-Hogg T, Tolmachova T, et al. Dual chemical probes enable quantitative system-wide analysis of protein prenylation and prenylation dynamics. *Nat Chem* 2019;11:552–61.
39. Berndt N, Hamilton AD, Sebt SM. Targeting protein prenylation for cancer therapy. *Nat Rev Cancer* 2011;11:775–91.
40. Stolze B, Reinhart S, Bullinger L, Frohling S, Scholl C. Comparative analysis of KRAS codon 12, 13, 18, 61, and 117 mutations using human MCF10A isogenic cell lines. *Sci Rep* 2015;5:8535.
41. Kiessling MK, Curioni-Fontecedro A, Samaras P, Atrott K, Cosin-Roger J, Lang S, et al. Mutant HRAS as novel target for MEK and mTOR inhibitors. *Oncotarget* 2015;6:42183–96.
42. Han JY, Oh SH, Morgillo F, Myers JN, Kim E, Hong WK, et al. Hypoxia-inducible factor 1alpha and antiangiogenic activity of farnesyltransferase inhibitor SCH66336 in human aerodigestive tract cancer. *J Natl Cancer Inst* 2005;97:1272–86.
43. Oh SH, Kim WY, Kim JH, Younes MN, El-Naggar AK, Myers JN, et al. Identification of insulin-like growth factor binding protein-3 as a farnesyl transferase inhibitor SCH66336-induced negative regulator of angiogenesis in head and neck squamous cell carcinoma. *Clin Cancer Res* 2006;12:653–61.
44. Yue X, Lin X, Yang T, Yang X, Yi X, Jiang X, et al. Rnd3/RhoE modulates hypoxia-inducible factor 1alpha/vascular endothelial growth factor signaling by stabilizing hypoxia-inducible factor 1alpha and regulates responsive cardiac angiogenesis. *Hypertension* 2016;67:597–605.
45. Saada-Bouazid E, Le Tourneau C. Beyond EGFR targeting in SCCHN: angiogenesis, PI3K, and other molecular targets. *Front Oncol* 2019;9:74.
46. Charvat S, Duchesne M, Parvaz P, Chignol MC, Schmitt D, Serres M. The up-regulation of vascular endothelial growth factor in mutated Ha-ras HaCaT cell lines is reduced by a farnesyl transferase inhibitor. *Anticancer Res* 1999;19:557–61.
47. White AC, Tran K, Khuu J, Dang C, Cui Y, Binder SW, et al. Defining the origins of Ras/p53-mediated squamous cell carcinoma. *Proc Natl Acad Sci U S A* 2011;108:7425–30.
48. He F, Melamed J, Tang MS, Huang C, Wu XR. Oncogenic HRAS activates Epithelial-to-mesenchymal transition and confers stemness to p53-deficient urothelial cells to drive muscle invasion of basal subtype carcinomas. *Cancer Res* 2015;75:2017–28.
49. Wend P, Wend K, Krum SA, Miranda-Carboni GA. The role of WNT10B in physiology and disease. *Acta Physiol* 2012;204:34–51.
50. Ho AL, Chau N, Bauman J, Bible K, Chintakuntlawar A, Cabanillas ME, et al. Preliminary results from a phase II trial of tipifarnib in squamous cell carcinomas (SCCs) with HRAS mutations. *Ann Oncol* 2018;29(suppl 8):viii372–99.

Molecular Cancer Therapeutics

Tipifarnib as a Precision Therapy for *HRAS*-Mutant Head and Neck Squamous Cell Carcinomas

Mara Gilardi, Zhiyong Wang, Marco Proietto, et al.

Mol Cancer Ther 2020;19:1784-1796. Published OnlineFirst July 29, 2020.

Updated version Access the most recent version of this article at:
doi:[10.1158/1535-7163.MCT-19-0958](https://doi.org/10.1158/1535-7163.MCT-19-0958)

Supplementary Material Access the most recent supplemental material at:
<http://mct.aacrjournals.org/content/suppl/2021/01/09/1535-7163.MCT-19-0958.DC1>

Cited articles This article cites 50 articles, 10 of which you can access for free at:
<http://mct.aacrjournals.org/content/19/9/1784.full#ref-list-1>

Citing articles This article has been cited by 2 HighWire-hosted articles. Access the articles at:
<http://mct.aacrjournals.org/content/19/9/1784.full#related-urls>

E-mail alerts [Sign up to receive free email-alerts](#) related to this article or journal.

Reprints and Subscriptions To order reprints of this article or to subscribe to the journal, contact the AACR Publications Department at pubs@aacr.org.

Permissions To request permission to re-use all or part of this article, use this link
<http://mct.aacrjournals.org/content/19/9/1784>.
Click on "Request Permissions" which will take you to the Copyright Clearance Center's (CCC) Rightslink site.